Applied Physics B (2018) 124:14
https://doi.org/10.1007/s00340-017-6884-7

Applied Physics B
Lasers and Optics

Isotope-selective ionization utilizing field-free alignment of isotopologues using a switched nanosecond laser pulse

Hiroshi Akagi[1] · Takayuki Kumada[2] · Tomohito Otobe[1] · Ryuji Itakura[1] · Hirokazu Hasegawa[3] · Yasuhiro Ohshima[4]

Received: 20 October 2017 / Accepted: 16 December 2017 / Published online: 22 December 2017

Abstract
We propose and numerically simulate a method of laser isotope separation based on field-free alignment of isotopologues, utilizing an intense "switched" nanosecond (ns) laser field which is slowly turned on and rapidly turned off at the peak with the falling time of 200 fs. The femtosecond (fs) laser-induced alignment of isotopologues including heavy isotopes is severely disturbed by ionization because of their small ionization potential. Our simulations for $I^{79}Br$ and $I^{81}Br$ isotopologues demonstrate that the switched ns laser field can make isotopologues well-aligned with the reduced ionization probability at the laser intensity [$I_0 = 2$ TW/cm^2 ($=2\times10^{12}$ W/cm^2)] which is an order-of-magnitude lower than a typical intensity ($I_0 = 20$ TW/cm^2) for field-free alignment induced by a fs laser field. In our simulations, I^iBr isotopologues ($i = 79$ or 81) aligned with the switched ns laser field are selectively ionized by an intense fs laser pulse at an appropriate time delay from the alignment pulse.

1 Introduction

An intense femtosecond (fs) laser pulse excites a molecule through the rotational Raman transitions, and creates a rotational wave packet in the molecule, which exhibits transient alignment and anti-alignment periodically with interval of its revival time [1–3]. Utilizing the field-free alignment induced by an intense fs laser pulse, we demonstrated isotope-selective ionization of $^{14}N_2$ and $^{15}N_2$ isotopologues [4]. In the demonstration, we shined an intense fs pulse with linear polarization (alignment pulse) to create rotational wave packets in these two isotopologues. At specific time delays after the alignment pulse irradiation, one isotopologue was aligned and the other one was anti-aligned due to difference between the revival times T_i^{rev} ($i = 14$ or 15). At one of the time delays, we shined another linearly-polarized intense fs pulse (ionization pulse) to ionize the isotopologues. Because of angular dependence of the N_2 ionization probability [5–10], ionization of the aligned isotopologue is enhanced, whereas that of the anti-aligned one is suppressed. Our experiment showed that the ion yield ratio R [$=I(^{15}N_2^+)$ / $I(^{14}N_2^+)$] could be controlled in the range of $R = 0.85$–1.22, by changing the time delay t_{delay} between the alignment and ionization pulses [4].

The molecular laser isotope separation (MLIS) method based on the field-free alignment is a strong candidate for an isotope separation method of heavy isotopes, because the isotope selectivity does not decrease significantly as isotope mass of isotopologues increases [11]. Our simulations demonstrated that the selectivity has only a small dependence on the isotope mass [11]. This feature is an advantage over the conventional MLIS methods, based on vibrational excitation induced by an infrared laser light with a narrow linewidth [12–14]. The selectivity in the vibrational excitation depends on vibrational frequency difference between isotopologues, which decreases as the isotope mass increases [15]. Thus, in the conventional MLIS methods, the selectivity decreases as the mass of isotopologues increases. Additionally, some groups have realized an MLIS method utilizing vibrational wave packet propagation [16–19]. In

✉ Hiroshi Akagi
akagi.hiroshi@qst.go.jp

1 Kansai Photon Science Institute, National Institutes for Quantum and Radiological Science and Technology (QST), 8-1-7 Umemidai, Kizugawa, Kyoto 619-0215, Japan

2 Materials Sciences Research Center, Japan Atomic Energy Agency, Tokai, Ibaraki 319-1195, Japan

3 Department of Integrated Sciences, Graduate School of Arts and Sciences, The University of Tokyo, Komaba, Meguro, Tokyo 153-8902, Japan

4 Department of Chemistry, School of Science, Tokyo Institute of Technology, 2-12-1 Ookayama, Meguro, Tokyo 152-8550, Japan

the method, the isotope selectivity originates from difference in time-evolution between vibrational wave packets. Time evolution makes the vibrational wave packets spatially separated in the vibrational coordinate due to difference in vibrational period ΔT^{vib}. However, the difference ΔT^{vib} also decreases as the isotope mass increases. For a binary mixture of homonuclear diatomic isotopologues ($^{\alpha}X_2$ and $^{\beta}X_2$), as an example, ΔT^{vib} is proportional to $\Delta m/(m_{\beta})^{1/2}$, where m_{β} is the atomic mass of $^{\beta}X$, and Δm is the difference between m_{β} and m_{α} ($\Delta m = m_{\beta} - m_{\alpha}$), as described in Ref [11]. This relation indicates that the time difference decreases as m_{β} increases, resulting in lowering of the selectivity.

To clearly separate the vibrational wave packets in the spatial coordinate, we need to wait for a number of vibrational recurrences until the wave packet of the heavier isotopologue delayed by a half of the vibrational period T^{vib} [16]. Additionally, the vibrational wave packets collapse and revive periodically due to the vibrational anharmonicity. The vibrational revival does not always coincide with the timing when the delay between the vibrational wave packets is equal to $T^{\mathrm{vib}}/2$ [16]. On the other hand, at the first revival of the rotational wave packets, the influence of the centrifugal distortion is small and the isotope selectivity is achieved at a reasonable level [11].

In the MLIS based on the field-free alignment, the isotope selectivity depends strongly on the degree of alignment of isotopologues. The degree of alignment can be improved by increasing the intensity of the fs alignment pulse [20–22]. However, the alignment improvement is restricted by non-resonant ionization [23–26]. An intense alignment pulse also causes the ionization, which degrades the isotope selectivity. Hence, the isotope selectivity cannot be improved significantly as the pulse intensity is increased. The restriction on the alignment improvement due to ionization is serious for isotopologues including heavy isotopes, because of its low ionization potential. Multiple pulse irradiation, that is, a train of fs alignment pulses also can improve the degree of alignment without increasing the pulse intensity [25, 27–30]. Actually, our experiments for $^{14}N_2$ and $^{15}N_2$ isotopologues demonstrated that a train of four fs pulses with the pulse interval of 125.7 ps ($= 15\ T_{14}^{\mathrm{rev}} = 14\ T_{15}^{\mathrm{rev}}$) creates rotational wave packets in the isotopologues exhibiting higher degree of alignment [31]. In this case, we obtained the higher isotope selectivity with R ranging from 0.49 to 2.00. Our numerical simulations showed that selectivity can be further improved by increasing a number of the fs alignment pulses to 12, which leads to the wider R range of 0.31–3.0 [31]. However, the selectivity can no longer be improved, when the number of pulses increases to more than 12. This is because the centrifugal distortion induces time-mismatch between the pulse train and the rotational revivals [28, 32, 33]. The other strategies using more elaborated pulse-shaping techniques can make molecules well-aligned at a reasonable laser intensity, as demonstrated theoretically [23, 24, 27, 30, 34–38] and experimentally [39, 40]. Some of them can align multiple isotopologues simultaneously [23, 30], possibly leading to the higher selectivity.

In the present work, we focus our attention on another field-free alignment method, in which we consider an intense nanosecond (ns) laser field with rapid turn off at the maximum field (Fig. 1a) [41, 42]. Hereafter, we call the shaped pulse the "switched" ns pulse. In the slowly turned-on laser field, a molecule exhibits a high degree of alignment along the laser electric field in an adiabatic manner. At the rapid turn off, a rotational wave packet is created in a nonadiabatic manner, exhibiting transient alignment and anti-alignment periodically in the temporal propagation (Fig. 1b). The switched ns pulse makes molecules well-aligned at a lower intensity [$I_0 \sim 1$ TW/cm^2 ($= 1 \times 10^{12}$ W/cm^2)] [43–45] than a typical intensity ($I_0 = 10$–100 TW/cm^2) of the fs alignment pulse. The feature of the alignment with the switched ns pulse is useful to reduce the ionization probability, and especially suitable for alignment of isotopologues including heavy isotopes.

We demonstrate theoretically isotope separation of $I^{79}Br$ and $I^{81}Br$ isotopologues aligned with a switched ns pulse, as an example. At a certain delay from the switched pulse, the isotopologues are irradiated with an intense fs pulse for the non-resonant ionization. We simulate the field-free alignment of the IBr isotopologues induced by the switched ns pulse that a laser pulse with 6-ns duration in full width at half maximum (FWHM) is truncated with the falling time

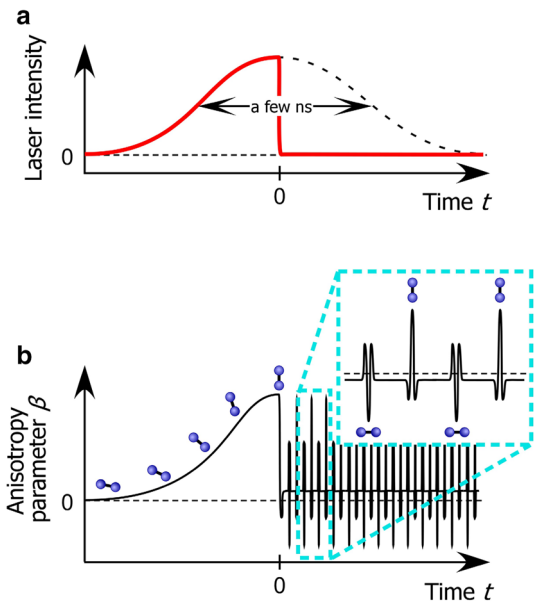

Fig. 1 Conceptual diagrams of the field-free alignment utilizing a ns laser field with rapid turn off; **a** Temporal profile of the laser field, and **b** time dependence of anisotropy parameter β with sketches of the molecular alignment

of ~200 fs. The degree of IBr alignment is compared with two results simulated for unshaped pulses: the IBr alignment induced by a fs pulse with 60-fs duration in FWHM, and that induced by a ps pulse with 3-ps duration. To evaluate the isotope selectivity and the required laser condition, ion yield ratio of the isotopologues, $R = I(\mathrm{I}^{81}\mathrm{Br}^+)/I(\mathrm{I}^{79}\mathrm{Br}^+)$, is calculated as a function of t_{delay} of the fs ionization pulse from the timing of the rapid turn off.

2 Computational details

We solve the time-dependent Schrödinger equation (TDSE) for time evolution of rotational wave packets in IBr isotopologues [31, 46]. The Hamiltonian is expressed by the field-free rotational one ${}^i\hat{H}_0$ for $\mathrm{I}^i\mathrm{Br}$ isotopologue ($i = 79$ or 81), and the interaction potential with the alignment laser field $\hat{H}_{\mathrm{ind}}(t)$ [1–3], as follows:

$$ {}^i\hat{H}(t) = {}^i\hat{H}_0 + \hat{H}_{\mathrm{ind}}(t). \tag{1}$$

An eigenenergy of the first term ${}^i\hat{H}_0$ at the rotational quantum number J is calculated by utilizing a set of Dunham-type parameters $Y_{k,l}$, including the quadratic and higher-order centrifugal distortion terms [47], as follows:

$$ {}^i\hat{H}_0 = \sum_{k,l} Y_{k,l}(1/2)^k[J(J+1)]^l. \tag{2}$$

The second term of Eq. (1) can be expressed using the temporal amplitude (envelop) of the laser electric field $E(t)$, and the angle between the molecular axis and the laser electric field direction θ, as follows:

$$ \hat{H}_{ind}(t) = -\frac{1}{4}E(t)^2(\alpha_{\parallel}\cos^2\theta + \alpha_{\perp}\sin^2\theta). \tag{3}$$

Here $\alpha_{\parallel}$ and $\alpha_{\perp}$ are the polarizabilities in the parallel and perpendicular directions to the IBr molecular axis, respectively. The laser electric field $E(t)$ of the switched ns pulse is defined as,

$$ E(t) = E_0 \exp[-2(\ln 2)(t/\tau_r)^2] \quad (t \leqslant 0), \tag{4a}$$

$$ E(t) = E_0 \exp[-2(\ln 2)(t/\tau_f)^2] \quad (t > 0), \tag{4b}$$

where the maximum electric field E_0 is set to be the experimentally realized value of 3.88×10^9 V m^{-1} ($I_0 = 2$ TW/cm^2) [45], and τ_{r} and τ_{f} represent the rising and falling times of the electric field. Here, we use $\tau_{\mathrm{r}} = 6$ ns, which is a typical value of a Nd:YAG laser output, and $\tau_{\mathrm{f}} = 200$ fs, which is almost the same as the experimental values [43–45]. The polarizabilities $\alpha_{\parallel}$ and $\alpha_{\perp}$ of IBr are calculated to be $\alpha_{\parallel} = 1.17 \times 10^{-39}$ C m^2 V^{-1} and $\alpha_{\perp} = 7.8 \times 10^{-40}$ C m^2 V^{-1}, by solving time-dependent Kohn–Sham (TD-KS) equation [48], which is the fundamental equation of the time-dependent density-functional theory (TD-DFT), with KLI-SIC exchange–correlation potential [49, 50]. The TDSE is solved numerically per time step of 2 fs, using the fourth-order Runge–Kutta method [51]. For comparison, the simulation using a 60-fs alignment pulse ($\tau_{\mathrm{r}} = \tau_{\mathrm{f}} = 60$ fs, 0.5-fs time step) with an order-of-magnitude higher intensity of $I_0 = 20$ TW/cm^2, and that using a 3-ps alignment pulse ($\tau_{\mathrm{r}} = \tau_{\mathrm{f}} = 3$ ps, 0.5-fs time step) with $I_0 = 20$ TW/cm^2 are performed in the same manner.

The degree of alignment is quantified using anisotropy parameter $\beta = 3\langle\cos^2\theta\rangle - 1$, where $\langle\cos^2\theta\rangle$ is the expectation value of $\cos^2\theta$. Here, the perfectly aligned, anti-aligned, and isotropic distributions have β values of 2, −1, and 0, respectively.

To obtain the ion yield ratio R [$= I(\mathrm{I}^{81}\mathrm{Br}^+)/I(\mathrm{I}^{79}\mathrm{Br}^+)$] as a function of time delay t_{delay}, the ion yield $I(\mathrm{I}^i\mathrm{Br}^+)$ is calculated for each IBr isotopologue, by utilizing the time-dependent angular distribution ${}^iP(\theta, t_{\mathrm{delay}})$ and the angular-dependent ionization probability $\Gamma(\theta)$, as follows:

$$ I(\mathrm{I}^i\mathrm{Br}^+) = \int_0^{\pi} {}^iP\left(\theta, t_{\mathrm{delay}}\right) \cdot \Gamma(\theta)\, \mathrm{d}\theta, \tag{5}$$

where ${}^iP(\theta, t_{\mathrm{delay}})$ is obtained as the square of the time-dependent rotational wavefunction. The ionization probability $\Gamma(\theta)$ of IBr caused by a fs laser field (16.2-fs duration in FWHM, $\lambda = 800$ nm, $I_0 = 15$ TW/cm^2) is simulated as a function of the angle θ between the molecular axis and the laser field direction. The simulation procedure has been reported in detail [52, 53]. Briefly, we solve the TD-KS equation [48] with KLI-SIC exchange–correlation potential [49, 50]. The out-going wave function, which corresponds to the ionization flux, is mimicked by the absorbing boundary condition [52]. To calculate the ion yield $I(\mathrm{I}^i\mathrm{Br}^+)$, we assume the ionization pulse with 60-fs duration. However, the simulation of the ionization probability is so time-consuming that $\Gamma(\theta)$ is calculated for the shorter pulse with 16.2-fs duration and is simply multiplied by 3.7 (= 60/16.2) to calculate $I(\mathrm{I}^i\mathrm{Br}^+)$.

3 Results

3.1 Field-free alignment

Figure 2a shows time dependence of anisotropy parameters β for IBr isotopologues (the rotational temperature of $T_{\mathrm{rot}} = 5$ K) when a switched 6-ns pulse with $I_0 = 2$ TW/cm^2 is used for the alignment. The two isotopologues behave in the same manner, excepting the revival times T_i^{rev} ($T_{79}{}^{\mathrm{rev}} = 294.0$ ps, $T_{81}{}^{\mathrm{rev}} = 298.6$ ps). For each isotopologue, β gradually increases in the time range of $t < 0$, and after the sudden decrease in the laser intensity at $t = 0$, it shows a spike-like

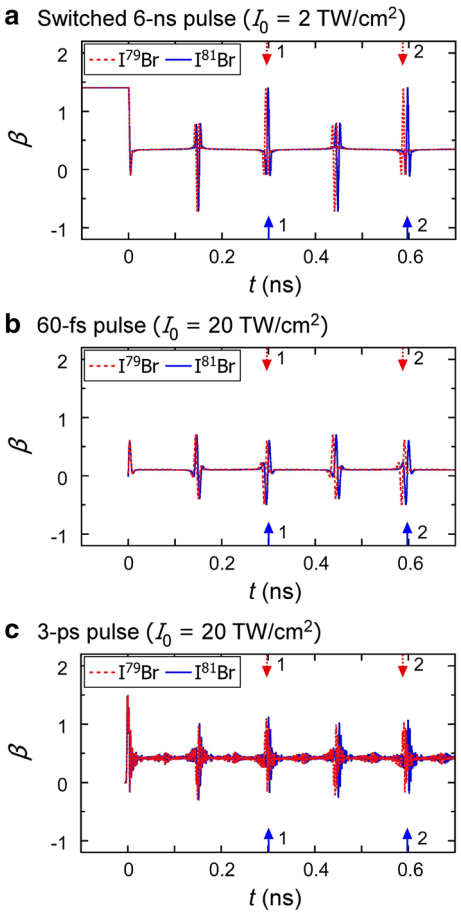

Fig. 2 **a** Time dependence of anisotropy parameters β for $I^{79}Br$ (red dashed curve) and $I^{81}Br$ (blue solid curve) isotopologues (T_{rot} = 5 K) when a switched ns pulse (τ_r = 6 ns, τ_f = 200 fs) with I_0 = 2 TW/cm^2 is used for the alignment. The down arrows with dotted stem indicate the revival times of $I^{79}Br$, and the up arrows indicate those of $I^{81}Br$. **b, c** Same as **a** for a 60-fs pulse ($\tau_r = \tau_f$ = 60 fs) with I_0 = 20 TW/cm^2, and for a 3-ps pulse ($\tau_r = \tau_f$ = 3 ps) with I_0 = 20 TW/cm^2, respectively

dip with two small side peaks at every half revival of $t = (n + 1/2)T_i^{rev}$ (n is an integer), and a spike-like peak with two small side dips at every full revival of $t = n\,T_i^{rev}$. These behaviors are the typical features of the field-free alignment induced by a switched ns pulse [41, 42]. The anisotropy parameter β varies in the range of −0.72 to 1.40 for each isotopologue. The variation range caused by the switched 6-ns pulse is twice as wide as that by a 60-fs pulse irradiation with an order-of-magnitude higher intensity of I_0 = 20 TW/cm^2 ($\beta = -0.49 \sim 0.70$), as shown in Fig. 2a, b.

It is known that the degree of alignment in the non-adiabatic regime (when the pulse duration Δt is much shorter than the rotational period T_i^{rev}) is maximized by the pulse energy. Quantum mechanical calculations have demonstrated that the non-adiabatic regime would remain unchanged if the laser pulse is chirped up to $\Delta t \sim T_i^{rev}/100$ [54]. For T_i^{rev} ~ 300 ps of IBr isotopologues, we can extend the duration

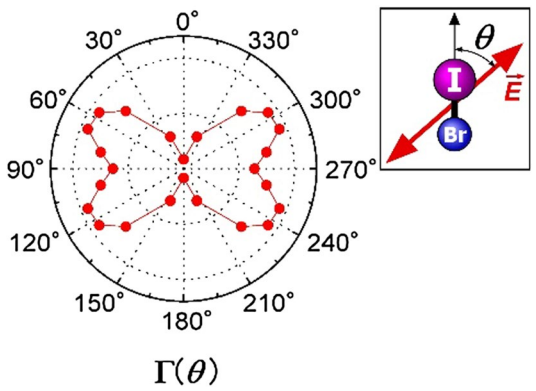

Fig. 3 Angular dependence of the ionization probability $\Gamma(\theta)$ of IBr obtained by solving the TD-KS equation (λ = 800 nm, I_0 = 15 TW/cm^2) [52, 53]

up to ~ 3 ps, 50 times longer than the 60-fs pulse. Figure 2c shows the result for a 3-ps pulse with I_0 = 20 TW/cm^2. The anisotropy parameter β ranges from −0.30 to 1.49, which is wider than that for the 60-fs pulse (Fig. 2b) due to its 50 times larger pulse energy. The maximum of 1.49 is larger than that for the switched 6-ns pulse (β = 1.40). However, the maximum appears at a short time delay of $t \sim 0.45$ ps, when the β curve of $I^{79}Br$ almost overlaps with that of $I^{81}Br$. The negligible difference will give us only a small isotope selectivity. Excepting the short delay range of $t < 10$ ps, β ranges from −0.30 to 1.10 for each isotopologue. The β range is narrower than that for the switched 6-ns pulse ($\beta = -0.72$ to 1.40) because, in the non-adiabatic regime, a single-pulse irradiation imposes a restriction on the achievable alignment [40, 55, 56]. These results indicate that the switched 6-ns pulse can induce a better IBr alignment than those induced by the unshaped pulses, in spite of its lower laser intensity.

3.2 Evaluation of the isotope selectivity

To evaluate the isotope selectivity, we simulate the ion yield for each I^iBr isotopologue (T_{rot} = 5 K) irradiated with the switched 6-ns pulse (I_0 = 2 TW/cm^2), followed by the 60-fs ionization pulse with I_0 = 15 TW/cm^2 as a function of time delay t_{delay} of the ionization pulse from the timing of the rapid turn off of the switched ns pulse. Here, angular dependence of ionization probability $\Gamma(\theta)$ shown in Fig. 3 is used in the simulation of the ion yield $I(I^iBr^+)$ represented by Eq. (5). The angular dependence shows a butterfly-like pattern, which implies that the ion yield decreases when IBr is aligned to the laser electric field, and the yield increases when IBr is anti-aligned. Figure 4a shows the ion yields $I(I^{79}Br^+)$ and $I(I^{81}Br^+)$ in the two ranges of $t_{delay} = -0.1 \sim 0.7$ ns, and 9.3 ~ 10.0 ns. In the former range, the first couple of full revivals of the two isotopologues shift

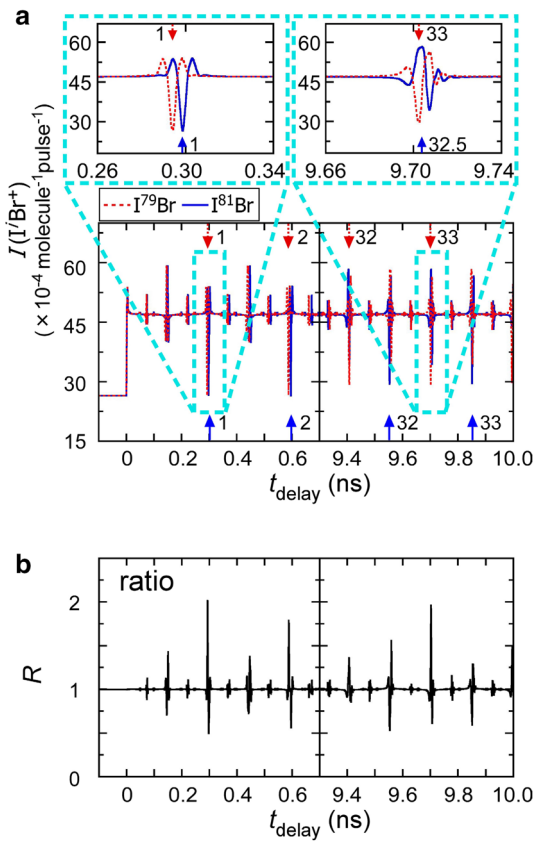

Fig. 4 **a** The simulated ion yields of $I^{79}Br^+$ (red dashed curve) and $I^{81}Br^+$ (blue solid curve), as a function of time delay t_{delay} in the two ranges of −0.1 to 0.7, and 9.3–10.0 ns. **b** The ratio R [$=I(I^{81}Br^+)/I(I^{79}Br^+)$] as a function of t_{delay}

slightly. In the latter range, a full revival of $I^{79}Br$ coincides with a half revival of $I^{81}Br$, and vice versa. Because of the alignment dependence of the ionization, $I(I^iBr^+)$ shows a peak at every half revival, and a dip at every full revival. In the delay range of 9.3 to 10.0 ns, the dips at the full revivals are smaller, and the peaks at the half revivals are slightly smaller than those in the delay range of −0.1 to 0.7 ns. These results are attributed to the centrifugal distortion effect, which leads to dephasing of the rotational wave packet. In addition to the half and full revivals, a small peak of $I(I^iBr^+)$ appears at every quarter revival of $t = (n+1/2)T_i^{rev}/2$, whereas no peak appears in β (Fig. 2a). At the quarter revivals, the wave packet shows a butterfly-like angular distribution ${}^iP(\theta)$, being similar with the ionization probability $\Gamma(\theta)$ shown in Fig. 3. The butterfly-like shape of ${}^iP(\theta)$ causes the increase of $I(I^iBr^+)$ at the quarter revival due to the large overlap with $\Gamma(\theta)$.

Figure 4b shows the ion yield ratio R [$=I(I^{81}Br^+)/I(I^{79}Br^+)$], in which several peaks and dips appear, demonstrating that the present approach works well as an MLIS method. The maximum is obtained to be $R_{max} = 2.01$ at $t_{delay} = 294.0$ ps, where the main dip of $I(I^{79}Br^+)$ at the first full revival coincides with the side peak of $I(I^{81}Br^+)$ preceding the main dip, as shown in left inset in Fig. 4a. The minimum is $R_{min} = 0.49$ at $t_{delay} = 298.4$ ps, where the main dip of $I(I^{81}Br^+)$ at the first full revival coincides with the side peak of $I(I^{79}Br^+)$ following the main dip (left inset in Fig. 4a).

A wide range of R is expected when a main peak of one isotopologue coincides with a main dip of the other one. This out-of-phase condition is realized when a half revival of one isotopologue coincides with a full revival of the other one [11, 57], that is, $(n+1/2)\,T_i^{rev} \approx n'\,T_j^{rev}$. The time delays for the out-of-phase condition are derived as:

$$t_{\text{out-of-phase}}(k) \approx (2k-1)T_{79}{}^{\text{rev}}T_{81}{}^{\text{rev}}/[2(T_{81}{}^{\text{rev}} - T_{79}{}^{\text{rev}})], \quad (6)$$

where $k = n' - n$ [11]. The ratio R around the shortest $t_{\text{out-of-phase}}(k=1) \approx 9.5$ ns is shown in the right panel of Fig. 4b. Although the temporally varying $I(I^{79}Br^+)$ and $I(I^{81}Br^+)$ are out-of-phase around $t_{delay} = 9.5$ ns (right panel of Fig. 4a), the selectivity is lower than that around the first revival; R at the peak is smaller than $R_{max} = 2.01$ at $t_{delay} = 294.0$ ps, and R at the dip is larger than $R_{min} = 0.49$ at $t_{delay} = 298.4$ ps. This situation is different from the N_2 isotope selective ionization [4, 31]. In the N_2 case, the higher selectivity is obtained at $t_{delay} \approx t_{\text{out-of-phase}}(k=1)$.

4 Discussion

4.1 Influence of ionization induced by alignment laser pulses

To achieve a high isotope selectivity, we should take care of not only enhancement of the alignment but also suppression of the ionization induced by the alignment pulse. Although the switched 6-ns pulse with an order-of-magnitude lower intensity will lead to a lower ionization rate than that of the 60-fs pulse (or the 3-ps pulse), we should take the pulse durations into account, because of the switched 6-ns pulse which is five (three) orders-of-magnitude longer than that of the 60-fs pulse (the 3-ps pulse). In the following estimation of the ionization probabilities, we assume a Ti:sapphire laser ($\lambda \sim 800$ nm, $\tau_r = \tau_f = 60$ fs) as an example of the unshaped pulses and a Nd:YAG laser ($\lambda \sim 1064$ nm, $\tau_r = 6$ ns, $\tau_f = 200$ fs) for the switched ns pulse. Here, we consider two limiting cases of nonlinear ionization, multiphoton and tunnel ionizations [58]. On the basis of the IBr ionization potential ($I_p = 9.79$ eV [59]), the IBr ionization requires seven photons at $\lambda \sim 800$ nm and 9 photons at $\lambda \sim 1064$ nm. In the multiphoton ionization limit, where the Keldysh's adiabaticity parameter γ ($= \sqrt{I_p/2U_p}$, where U_p is the ponderomotive energy) $\gg 1$, the probability can be estimated using the

ionization cross section $\sigma(\lambda)$, the laser intensity I_0, and the pulse duration Δt, as:

$$P_{\text{ion}}(\lambda) \approx \sigma(\lambda) {I_0}^N \Delta t, \quad (7)$$

where N is the required number of photons. As far as we know, $\sigma(\lambda)$ of IBr is not available at $\lambda = 800$ and 1064 nm. Therefore, in the present estimation, we suppose that $\sigma(1064\text{ nm}) = \sigma(800\text{ nm})$. As the intensity I_0 of 1064-nm pulse is decreased by one order-of-magnitude, the ionization rate ($= \sigma(\lambda)\ {I_0}^N$) is decreased by nine orders-of-magnitude. Considering the switched 6-ns pulse being five orders-of-magnitude longer than the 60-fs pulse, $P_{\text{ion}}(\lambda)$ induced by the switched 6-ns pulse with $I_0 = 2$ TW/cm^2 is four (= 9–5) orders-of-magnitude lower than that induced by the 60-fs pulse with $I_0 = 20$ TW/cm^2. On the basis of this order estimation, it is obvious that $P_{\text{ion}}(\lambda)$ induced by the switched 6-ns pulse with a realistic intensity is lower than that induced by the 60-fs pulse, unless $\sigma(1064\text{ nm})$ is four or more orders-of-magnitude larger than $\sigma(800\text{ nm})$. In the tunnel ionization limit, where $\gamma << 1$, we use the simple ADK theory [60] to estimate the ionization rate. The ADK rate of IBr ionization at $I_0 = 2$ TW/cm^2 is sixteen orders-of-magnitude lower than that at $I_0 = 20$ TW/cm^2, independently of the wavelength. Taking the pulse durations into account, we estimate that the ionization probability induced by the switched 6-ns pulse is 11 (= 16–5) orders-of-magnitude lower than that induced by the 60-fs pulse. These estimations for the two limiting cases suggest that the ionization induced by the switched 6-ns pulse ($\gamma = 6.8$ for 1064-nm pulse with $I_0 = 2$ TW/cm^2) also has a lower probability than that induced by the 60-fs pulse ($\gamma = 2.9$ for 800-nm pulse with $I_0 = 20$ TW/cm^2). Therefore, we expect that the present approach using the switched ns pulse works effectively for isotope separation of heavy isotopes.

4.2 Rotational dephasing

The lower selectivity of IBr at $t_{\text{delay}} \approx t_{\text{out-of-phase}}(k = 1)$ (Fig. 4b) is due to the small dips and the small peaks in each $I(\text{I}^i\text{Br}^+)$. As shown by the dashed curves in insets in Fig. 4a, the main dip shape of $I(\text{I}^{79}\text{Br}^+)$ observed at the first full revival (left inset) is not identically reproduced at the 33rd full revival (right inset), where $I(\text{I}^{79}\text{Br}^+)$ shows an asymmetric "chirped" structure [61]. The chirped structure is also observed at the 33rd half revival of $I(\text{I}^{81}\text{Br}^+)$ (solid curve in the right inset). These chirped structures cause the lower contrast in each $I(\text{I}^i\text{Br}^+)$ (right inset in Fig. 4a), resulting in the lower selectivity at $t_{\text{delay}} = t_{\text{out-of-phase}}(k = 1) \approx 9.5$ ns (Fig. 4b).

These chirped structures imply serious dephasing of the rotational wave packet, which is a consequence of the centrifugal distortion effect [61]. However, centrifugal distortion effect of IBr is smaller than that of N_2. In Table 1, we compare a ratio D_0/B_0 of I^{79}Br [47] to that of $^{14}\text{N}_2$ [62], because the ratio is a nice index of the centrifugal distortion effect *per* revival [32, 33]. Here, D_0 and B_0 are the centrifugal distortion and rotational constants of the vibrational ground state, respectively. Actually, the ratio D_0/B_0 of I^{79}Br is an order-of-magnitude smaller than that of $^{14}\text{N}_2$, implying a smaller IBr dephasing at $t_{\text{delay}} \sim T_i^{\text{rev}}$.

Table 1 Rotational constant B_0 and ratio D_0/B_0 of the centrifugal distortion constant to B_0

	B_0 (cm^{-1})	$D_0/B_0 \times 10^6$
$^{14}\text{N}_2$ [62]	1.99	2.89
I^{79}Br [47]	0.0567	0.180

Rotational constants are taken from [47, 62]

The rotational dephasing of IBr at $t_{\text{delay}} \approx t_{\text{out-of-phase}}(k = 1)$ results from the following two factors: the wide rotational state distribution, and the large n and n' satisfying $t_{\text{delay}} \approx t_{\text{out-of-phase}}(k = 1)$. We discuss how the dephasing is affected by the two factors, comparing the IBr case with the N_2 case.

First, IBr has a two orders-of-magnitude smaller B_0 than N_2, as listed in Table 1. As far as T_{rot} is the same, the rotational state distribution of IBr is wider than that of N_2. At $T_{\text{rot}} = 5$ K, as an example, *ca.* 0.9 of $^{14}\text{N}_2$ molecules populate only in the $J = 0$ and $J = 1$ rotational levels, whereas *ca.* 0.9 of I^{79}Br molecules populate in the $J = 0 \sim 11$ levels. The centrifugal distortion effect quadratically increases as J increases [63]. Hence, the centrifugal distortion at $J = 11$ is two orders-of-magnitude larger than that at $J = 1$. Although D_0/B_0 of IBr is one order-of-magnitude smaller than that of N_2, IBr in the $J = 11$ level has, in total, an order-of-magnitude larger effect than N_2 in the $J = 1$, resulting in the larger dephasing of IBr.

Next, n (= 32) and n' (= 33) used in IBr are four times as large as those ($n = 8$, $n' = 7$) in N_2 [4]. In spite of the smaller dephasing *per* revival, the larger numbers of the revivals enhance the effect, resulting in the larger dephasing of IBr at $t_{\text{delay}} \approx t_{\text{out-of-phase}}(k = 1)$.

Both these two factors should contribute to the rotational dephasing of IBr observed at $t_{\text{delay}} \approx t_{\text{out-of-phase}}(k = 1)$. Isotopologues including heavy isotopes commonly have these two factors, the wide rotational state distribution and the large n and n'. When we apply the present MLIS method for heavy isotopes, serious dephasing will be observed at $t_{\text{delay}} \approx t_{\text{out-of-phase}}(k = 1)$. Therefore, the delay range around the first revival will provide higher isotope selectivity.

5 Conclusion and outlook

In the present study, we proposed an MLIS method based on field-free alignment of isotopologues induced by a switched ns laser pulse, as a strong candidate for an isotope

separation method of heavy isotopes. To demonstrate how the method works effectively for heavy isotopes, we performed the numerical simulations. Our simulations for IBr isotopologues ($T_{rot} = 5$ K) showed that a switched 6-ns laser pulse with $I_0 = 2$ TW/cm^2 can induce the better alignment with its variation range of β being wider than those obtained by unshaped pulses ($\Delta t = 60$ fs or 3 ps) with an order-of-magnitude higher intensity of $I_0 = 20$ TW/cm^2. This simulated result means that we can make isotopologues including heavy isotopes well-aligned with the switched ns pulse. Although the heavy isotopologues are easily ionized due to their low ionization potentials, the switched ns pulse can suppress the ionization probability significantly. Hence, the switched ns pulse has a significant advantage for isotope separation of heavy isotopes.

Additionally, we simulated the ion yield ratio R [$= I(I^{81}Br^+)/I(I^{79}Br^+)$] of the IBr isotopologues for the ionization caused by the fs ionization pulse at $I_0 = 15$ TW/cm^2, utilizing the ionization probability $\Gamma(\theta)$ shown in Fig. 3. The ratio varied in the range of 0.49–2.01, as a function of t_{delay} between the switched pulse and the fs ionization pulse. The R variation demonstrates the effectiveness of the present method utilizing the switched ns pulse.

The present MLIS utilizing a switched ns pulse can be applied to the other isotopologues by simply tuning the time delay, because the method does not use any resonance transitions [4, 31]. This fact means that we do not have to tune the laser wavelength, which makes a contrast to conventional laser isotope separation (LIS) methods, including conventional MLIS [12–14] and atomic vapor LIS methods [64, 65], where a tunable laser is needed to utilize isotope shift of resonant excitation. This advantage allows us to easily apply the present method to a wider variety of isotopes, including heavy isotopes.

Acknowledgements We would like to thank Professor Y. Ohtsuki and Professor I. Averbukh for their helpful comments and suggestions about the methods of field-free alignment. The present work was financially supported in part by JSPS KAKENHI (Grant Numbers 23656594, 26289367, and 17H03525), and by the Consortium for Photon Science and Technology.

References

1. H. Stapelfeldt, T. Seideman, Rev. Mod. Phys **75**, 543 (2003)
2. T. Seideman, E. Hamilton, Adv. At. Mol. Opt. Phys. **52**, 289 (2006)
3. Y. Ohshima, H. Hasegawa, Int. Rev. Phys. Chem. **29**, 619 (2010)
4. H. Akagi, T. Kasajima, T. Kumada, R. Itakura, A. Yokoyama, H. Hasegawa, Y. Ohshima, Appl. Phys. B **109**, 75 (2012)
5. I.V. Litvinyuk, K.F. Lee, P.W. Dooley, D.M. Rayner, D.M. Villeneuve, P.B. Corkum, Phys. Rev. Lett. **90**, 233003 (2003)
6. A.S. Alnaser, S. Voss, X.-M. Tong, C.M. Maharjan, P. Ranitovic, B. Ulrich, T. Osipov, B. Shan, Z. Chang, C.L. Cocke, Phys. Rev. Lett. **93**, 113003 (2004)
7. D. Pavičić, K.F. Lee, D.M. Rayner, P.B. Corkum, D.M. Villeneuve, Phys. Rev. Lett. **98**, 243001 (2007)
8. X.M. Tong, Z.X. Zhao, C.D. Lin, Phys. Rev. A **66**, 033402 (2002)
9. T. Otobe, K. Yabana, J.-I. Iwata, Phys. Rev. A **69**, 053404 (2004)
10. D.A. Telnov, S.-I. Chu, Phys. Rev. A **79**, 041401(R) (2009)
11. H. Akagi, H. Ohba, K. Yokoyama, A. Yokoyama, K. Egashira, Y. Fujimura, Appl. Phys. B **95**, 17 (2009)
12. V.S. Letokhov, Nature **277**, 605 (1979)
13. R.D. McAlpine, D.K. Evans, Adv. Chem. Phys. **60**, 31 (1985)
14. V.S. Letokhov, Appl. Phys. B **46**, 237 (1988)
15. V.S. Letokhov, *Nonlinear Laser Chemistry. Multi-Photon Excitation*, Chap. 2. (Springer, Berlin, 1983)
16. I.S. Averbukh, M.J.J. Vrakking, D.M. Villeneuve, A. Stolow, Phys. Rev. Lett. **77**, 3518 (1996)
17. A. Lindinger, C. Lupulescu, M. Plewicki, F. Vetter, A. Merli, S.M. Weber, L. Wöste, Phys. Rev. Lett. **93**, 033001 (2004)
18. A. Lindinger, C. Lupulescu, F. Vetter, M. Plewicki, S.M. Weber, A. Merli, L. Wöste, J. Chem. Phys. **122**, 024312 (2005)
19. B. Schäfer-Bung, V. Bonačić-Koutecký, F. Sauer, S.M. Weber, L. Wöste, A. Lindinger, J. Chem. Phys. **125**, 214310 (2006)
20. F. Rosca-Pruna, M.J.J. Vrakking, Phys. Rev. Lett. **87**, 153902 (2001)
21. F. Rosca-Pruna, M.J.J. Vrakking, J. Chem. Phys. **116**, 6567 (2002)
22. F. Rosca-Pruna, M.J.J. Vrakking, J. Chem. Phys. **116**, 6579 (2002)
23. S. Guérin, A. Rouzée, E. Hertz, Phys. Rev. A **77**, 041404(R) (2008)
24. A. Rouzée, E. Hertz, B. Lavorel, O. Faucher, J. Phys. B **41**, 074002 (2008)
25. J.P. Cryan, P.H. Bucksbaum, R.N. Coffee, Phys. Rev. A **80**, 063412 (2009)
26. R. Itakura, H. Hasegawa, Y. Kurosaki, A. Yokoyama, Y. Ohshima, J. Phys. Chem. A **114**, 11202 (2010)
27. H. Abe, Y. Ohtsuki, Phys. Rev. A **83**, 053410 (2011)
28. J. Floβ, I.S. Averbukh, Phys. Rev. A **86**, 021401(R) (2012)
29. S. Zhdanovich, C. Bloomquist, J. Floβ, I.S. Averbukh, J.W. Hepburn, V. Milner, Phys. Rev. Lett. **109**, 043003 (2012)
30. K. Nakashima, M. Yoshida, T. Nakajima, Y. Ohtsuki, Mol. Phys. **115**, 1730 (2017)
31. H. Akagi, T. Kasajima, T. Kumada, R. Itakura, A. Yokoyama, H. Hasegawa, Y. Ohshima, Phys Rev. A **91**, 063416 (2015)
32. J. Floβ, I.S. Averbukh, Phys. Rev. Lett. **113**, 043002 (2014)
33. J. Floβ, I.S. Averbukh, J Phys. Chem. A **120**, 3206 (2016)
34. C. Siedschlag, O.M. Shir, T. Bäck, M.J.J. Vrakking, Opt. Commun. **264**, 511 (2006)
35. E. Hertz, A. Rouzée, S. Guérin, B. Lavorel, O. Faucher, Phys. Rev. A **75**, 031403(R) (2007)
36. K. Nakagami, Y. Mizumoto, Y. Ohtsuki, J. Chem. Phys. **129**, 194103 (2008)
37. S. Zhang, C. Lu, T. Jia, Z. Sun, J. Qiu, J. Chem. Phys. **135**, 224308 (2011)
38. S. Xu, Y. Yao, C. Lu, J. Ding, T. Jia, S. Zhang, Z. Sun, Phys. Rev. A **89**, 053420 (2014)
39. T. Suzuki, Y. Sugawara, S. Minemoto, H. Sakai, Phys. Rev. Lett. **100**, 033603 (2008)
40. O. Ghafur, A. Rouzée, A. Gijsbertsen, W.K. Siu, S. Stolte, M.J.J. Vrakking, Nat. Phys. **5**, 289 (2009)
41. Z.-C. Yan, T. Seideman, J. Chem. Phys. **111**, 4113 (1999)
42. T. Seideman, J. Chem. Phys. **115**, 5965 (2001)
43. J.G. Underwood, M. Spanner, M.Y. Ivanov, J. Mottershead, B.J. Sussman, A. Stolow, Phys. Rev. Lett. **90**, 223001 (2003)
44. B.J. Sussman, J.G. Underwood, R. Lausten, M.Y. Ivanov, A. Stolow, Phys. Rev. A **73**, 053403 (2006)
45. A. Goban, S. Minemoto, H. Sakai, Phys. Rev. Lett. **101**, 013001 (2008)
46. H. Hasegawa, Y. Ohshima, Phys. Rev. A **74**, 061401(R) (2006)

47. T. Yukiya, N. Nishimiya, M. Suzuki, J. Mol. Spectrosc. **214**, 132 (2002)
48. E. Runge, E.K.U. Gross, Phys. Rev. Lett. **52**, 997 (1984)
49. X.-M. Tong, S.-I. Chu, Phys. Rev. A **57**, 855 (1998)
50. K. Yabana, G.F. Bertsch, Phys. Rev. B **54**, 4484 (1996)
51. W.H. Press, S.A. Teukolsky, W.T. Vetterling, B.P. Flannery, *Numerical Recipes in C. The Art of Scientific Computing*, 2nd edn. (Cambridge University Press, Cambridge, 1992)
52. T. Nakatsukasa, K. Yabana, J. Chem. Phys. **114**, 2550 (2001)
53. X. Chu, S.-I. Chu, Phys. Rev. A **64**, 063404 (2001)
54. R. Torres, R. de Nalda, J.P. Marangos, Phys. Rev. A **72**, 023420 (2005)
55. M. Leibscher, I.S. Averbukh, H. Rabitz, Phys. Rev. Lett. **90**, 213001 (2003)
56. M. Leibscher, I.S. Averbukh, H. Rabitz, Phys. Rev. A **69**, 013402 (2004)
57. S. Fleischer, I.S. Averbukh, Y. Prior, Phys. Rev. A **74**, 041403(R) (2006)
58. L.V. Keldysh, Sov. Phys. JETP **20**, 1307 (1965)
59. B.R. Higginson, D.R. Lloyd, P.J. Roberts, Chem. Phys. Lett. **19**, 480 (1973)
60. N.B. Delone, V.P. Krainov, Phys. Uspekhi **41**, 469 (1998)
61. P.W. Dooley, I.V. Litvinyuk, K.F. Lee, D.M. Rayner, M. Spanner, D.M. Villeneuve, P.B. Corkum, Phys. Rev. A **68**, 023406 (2003)
62. R.J. Le Roy, Y. Huang, C. Jary, J. Chem. Phys. **125**, 164310 (2006)
63. G. Herzberg, *Molecular Spectra and Molecular Structure Volume I. Spectra of Diatomic Molecules*, 2nd edn. (Van Nostrand Reinhold, New York, 1950)
64. P.A. Bokhan, V.V. Bochanov, N.V. Fateev, M.M. Kalugin, M.A. Kazaryan, A.M. Prokhorov, D.E. Zakrevskii, *Laser Isotope Separation in Atomic Vapor* (Wiley, New York, 2006)
65. C.R. Locke, T. Kobayashi, T. Fujiwara, K. Midorikawa, Appl. Phys. B **123**, 240 (2017)